

## Reducing Erodibility of Earthen Levee Using Engineered Flood Wall Sections

Chung R. Song<sup>1</sup> M. ASCE, Jinwon Kim<sup>2</sup> S. M. ASCE, Ge Wang<sup>3</sup> and Alexander, H.-D. Cheng<sup>4</sup>  
M. ASCE

<sup>1</sup>Assistant Professor, Department of Civil Engineering, University of Mississippi, Carrier 218, University, MS 38677; Tel.: 662-915-1646; E-mail: [csong@olemiss.edu](mailto:csong@olemiss.edu)

<sup>2</sup>Graduate Assistant, Department of Civil Engineering, University of Mississippi, Carrier 121L, University, MS 38677; E-mail: [jkim3@olemiss.edu](mailto:jkim3@olemiss.edu)

<sup>3</sup>Research Assistant Professor, Department of Civil Engineering, University of Mississippi, Carrier 121J, University, MS 38677; E-mail: [gewang@olemiss.edu](mailto:gewang@olemiss.edu)

<sup>4</sup>Professor and Chair, Department of Civil Engineering, University of Mississippi, Carrier 203, University, MS 38677; Tel.: 662-915-5362; E-mail: [acheng@olemiss.edu](mailto:acheng@olemiss.edu)

### Abstract

Erosion was one of the major causes for the failure of New Orleans levee system during Hurricane Katrina (IPET, 2007). The Protection of flood walls from erosion failure can be performed in many different ways. This study conducted an experimental study to develop the protective surface structure for the flood wall which can reduce the erosion energy of the plunging water before the water hits the levee materials, so the soil erosion is reduced. The test results are also compared to hydrodynamics simulations using FLOW3D. This study revealed that the erosion resistance of levee can be substantially reduced by providing protective structures at the surface of the flood walls. An effectively designed cross section could reduce the erosion depth as much as 40% in this study.

## **Introduction**

The ability of levees to withstand overtopping and associated erosion varied significantly for levees in New Orleans during hurricane Katrina (Briaud et al. 2008). The overtopped areas where the levees were constructed with rolled clayey materials (such as the soils at Orleans Canal) hardly experienced the erosion. Some other areas where the levees were constructed with silty or sandy materials (such as the soils at 17<sup>th</sup> St. Canal) experienced the severe erosion as shown in Fig.1.

### **Fig.1 goes to here**

By implicit design principles, earthen levees and dams are not expected to be overtopped. Overtopping situation of earthen levees typically means the failure. But, occasional severe weather condition brings unprecedented incidents such as the heavy rain and wind, and the levees may be overtopped consequently. Therefore, it is logical to secure a certain level of “resiliency” against the overtopping failure of earthen levees, so that the failure of the levee is prevented or delayed.

To design an erosion proof levee system, one may increase the overall height and width of an earthen levee. However, this indispensable principle is not a viable option in developed areas such as New Orleans – raising the levee height requires the widening the levee base and it may cause the intervention in ownerships of private lands. Building and raising a flood wall can be an alternative option. Just raising the elevation of flood wall without proper reinforcement may cause an overall stability problem for the flood wall and support system. A third option would be covering the erodible material by providing erosion-proof coats at the soil surface; this technique

is reported as early as 1929 by Shaw. Covering the levee using man made materials, historically, caused the environmental and aesthetic issues (Henderson, 1986; Comoss, 2002). A fourth option would be retrofitting the floodwall so that it can reduce the erosive energy of the overtopping water by itself to an acceptable degree. This option will not completely prevent the erosion, but it may provide reasonable protection for many soils with reasonable cost, or it can be used in combination with another method such as the environmentally friendly surface protection technique.

This study conducted experimental and theoretical researches for developing a flood wall section that can reduce the erosive energy of the overtopping water.

### **Erosion Test Bed**

The majority of soil erosion research had been conducted for the surface erosion caused by shearing flow such as the case of dam spillways (Hanson, 1991; Hanson and Robinson, 1993; Hunt et al. 2004, Chen and Anderson, 1986; Dodge, 1988; AlQaser and Ruff, 1993; Coleman et al. 2002) and scour around bridge abutments (Briaud et al. 1999). Typical erosion measurements in the laboratory are conducted using the jet erosion device by Hanson (2004), rotating cylinder apparatus proposed Moore and Masch (1962), drill hole apparatus by Rohan et al. (1986), and erosion function apparatus by Briaud et al. (2001). However, little work has been conducted on the plunging erosion (or impact erosion) at the backside of the flood walls. The general mechanisms of plunging water driven erosion may be quite different from the shear-stress driven erosion, because plunging water provides the oscillating normal and shear stresses rather than the continuously applied shear stress to the soils. Another uniqueness of the plunging water from the

flood wall is that it is narrow and long. To reproduce these field conditions in the lab, a unique testing bed is manufactured at The University of Mississippi.

A UMETB (University of Mississippi Erosion Testing Bed) is developed to simulate the soil erosion caused by the plunging water from the flood wall in New Orleans. The physical scale of UMETB is relatively large compared to conventional apparatus such as the jet test developed by Hanson et al (2004) and EFA (Erosion Function apparatus) by Briaud (2001). The UMETB consists of a nozzle, specimen box, two water containers, and five pumps. The flow rate is controlled using three 1/3 HP submersible sump pumps (Flotec, Model 030F07D). The three pumps in the inner water tank (ACE Roto-Hold) are connected to the 3.81 cm (1.5 inch) diameter circular pipes. Then, the pipes are all connected to a larger diameter collection pipe with 7.62 cm (3 inch) diameter. At the end of the larger diameter collection pipe the nozzle that has narrow width and long length is attached. The plunging water is driven through the nozzle with the designated flow rate (28.9 k liter/hr.). The details of the nozzle are shown in Fig. 2 (c).

**Fig 2 goes to here**

The soil is placed in the specimen box which has 38.6 cm × 20.8 cm × 12.8 cm dimensions, as shown in Figure 2. The specimen box has 1 cm × 1cm grid at the side so that the scour depth can be recorded via a video camera (Sony HDR SR-12). A plate vertically mounted at one end of the specimen box represents a flood wall. The nozzle and specimen box are made of 1.8 cm thickness transparent acrylic plate so that it is easy to monitor the scour depth, shape and flow condition. Additionally, the two ½ HP submersible sump pumps (Flotec, Model No. 030E07M) is installed at the outside water container (ACE Roto-Hold) for recirculation of the water into the inside tank so that a continuous supply of large amount of water is possible.

The ASTM 20-30 ottawa sand purchased from U.S. Silica company (Ottawa, IL) is used for the UMETB test. The sand specimen is loosely packed and fully saturated as the sample is submerged in the water for more than 2 days. The uniform C-190 sand is selected because it is highly erodible, properties are well known, and the input variables for hydrodynamical analysis are easy to determine.

### **Test Procedure**

The step-by-step procedure for the UMETB test is as follows:

- 1) Place the specimen box on a table. Spread the dry soil specimen into the test box using a small shovel. To acquire the constant compaction efforts, the drop height of the soil is kept at 1cm. The resulting void ratio is 0.67.
- 2) After filling the specimen box with the soil, water is gently introduced to saturate the soil without disturbance.
- 3) Mount the specimen box on the test bench so that the planar nozzle can be placed.
- 4) Adjust the nozzle height so that the nozzle touches the top of the flood wall and the water flows smoothly along the wall.
- 5) Mount and manually focus the video camera to record the erosion profile.
- 6) Turn on three pumps simultaneously to supply the water in the nozzle.

- 7) To maintain the constant flow rate from the nozzle before the initiation of the erosion test, the test box is covered by a plate and the pumps are allowed to achieve the constant flow rate (3sec. was good enough).
- 8) The video camera is turned on.
- 9) After confirming the constant flow rate that is visually recognizable, the plate is removed rapidly.
- 10) After the test, the recorded video (standard definition image quality) images are used for analyzing the erosion profile. In this study, PMB (Picture Motion Browser) supplied by the manufacture of the video camera is used.

### **Types of Model Flood Walls**

In this study, five different types of flood walls are tested. Each type has a different shape. The schematic shapes of each case are shown in Fig. 3. The case (A) represents the original flood wall shape that is shown in Fig. 4. In order to reduce or dissipate the kinetic energy of the plunging water, a 1cm by 1cm acrylic strip is attached to the flood wall for cases (B) and (C). For case (D), the 'L' shape of the strip is attached to the bottom of plate while two rows of 1cm by 1cm blocks are attached on the floodwall with zigzag pattern for case (E).

**Fig. 3 goes to here**

**Fig. 4 goes to here**

## Test Results

To check the validity of shutter speed 30 fps of the video camera, two different shutter speeds (30 fps and 120 fps) are tested. The captured still images using the software, PMB (Picture Motion Browser), from the recorded video are analyzed at 0.33 sec for 30 fps and at 0.08 sec for 120 fps intervals. The test results show the negligible difference between the two is shown in Fig. 5-c, 5-d and Table 1. Therefore, the standard shutter speed, 30 fps, is used in this study for the rest of the tests.

The maximum eroded depth for the case (A) is 12.8cm and it is the same as the depth of the specimen box. It indicates that the erosion of the specimen can be continued if the specimen box is deeper. However, this study kept the depth of specimen box due to the weight of the specimen (about 234N or 53 lb). Case (B), the one with strip attached 1.4 cm from the bottom, shows the ultimate erosion depth 9.9 cm which is lower than that of case (A). However, it is noted that the erosion reducing performance of case (B) is more than 4.8 cm recalling that case (A) did not reach the true ultimate condition. Case (C), the one with strip attached at the very bottom, shows a similar behavior as case (B) with the ultimate erosion depth 10.1 cm. Therefore the location of the strip seems not a major factor for erosion reducing performance. Case (D), the one with L shaped strip attached at the very bottom, shows a similar erosion behavior to cases (B) and (C). But it also shows a unique behavior. When the width of the L shape was increased to 2.0 cm, a substantial amount of the plunging water reflected from the L strip to outside the specimen box. The reflected water in real life may causes a secondary erosion, therefore the application of energy dissipating strips should be designed with this behavior in mind.

Apart from the erosion depth, the time to reach the ultimate erosion equilibrium is also significantly improved when we used the energy dissipating strips. From Fig. 5 and Table 1, case (A) took 1.7 seconds while cases (B), (C), (D) and (E) took 2.7 to 2.8 seconds. Again it is noted case (A) did not reach the ultimate equilibrium yet. When one compares the time to reach 10 cm erosion depth, that is the ultimate erosion depth for (B), (C), (D) and (E), case (A) took only 0.7 seconds that is much quicker than other cases. If the earthen levee is not erosion proof, that is the case in most real life conditions, the erosion time is critical to secure the evacuation time for residents. Through these results, it is clear that providing properly designed energy dissipation strips or blocks may reduce the erosion potential of levees significantly.

**Fig. 5 goes to here**

### **Verification with Numerical Simulation**

With the prompt development of modern computer technology and computational methods, nowadays, numerical simulations are playing more and more an important role in various engineering and research fields since they are economic, easy to manipulate, and the most important outcomes are that more detail insights into the physical process are easily to capture, and innovative explorations are convenient to proceed.

Erosion by overtopping flow is a very complex physical problem since it contains not only the dynamically evolving free surface flow structure above the soil surface, but also the complicate time-dependant interaction between the soil/flow media. Thus, a good numerical model is acquired to accurately solve these two challenging parts simultaneously.

In the present paper the above-made experimental results are verified with the numerical simulation using a hydrodynamics simulation software FLOW3D, coded by Flow Science Inc. USA. FLOW3D is developed to be capable of predicting not only the free surface flow produced by the overtopping water, but also the three dimensional erosion and transportation of packed and suspended sediment. The sediment scour model integrated in FLOW3D is an empirical approach of predicting fluid/solid interface, which means the sediment is not modeled as individual particles because such an approach would be computationally very intensive for most practical problems. Using FLOW3D, the sediment and erosion process is modeled with a continuum approach where the concentration of sediment is tracked. This concentration can vary from being completely packed to completely dilute. The erosion mode in FLOW3D consists of two basic components: drifting and lifting. Drifting acts on the sediment that is suspended in the flow; gravity, along with other body forces, causes the settling of the sediment. Lifting takes place only at the interface between the packed sediment and fluid and where the local shear stress imposed by the liquid on the bed interface exceeds a critical value. The amount of lifting is proportional to the shear stress. In conjunction with the drifting and lifting models, a drag model is used to mimic the solid-like behavior of the sediment in regions where its concentration exceeds a cohesive solid fraction; they are calculated as a function of the sediment concentration.

**FLOW3D** utilizes the following momentum equations for erosion/sedimentation analysis.

*Momentum equation:*

$$\frac{\partial \bar{u}}{\partial t} + \bar{u} \bullet \nabla \bar{u} = -\nabla p + \nabla \bullet \bar{\tau} + \bar{g} - K\bar{u} \quad (1)$$

where  $\bar{u}$ ,  $\bar{\tau}$  and  $\bar{g}$  are, respectively, the local velocity, fluid shear stress and gravity.  $p$  is pressure;  $K$  is the drag coefficient, a function of the solid volume fraction, and can be determined as follows (Brethour, 2006):

$$K = \begin{cases} 0 & \text{if } f_s < f_{s,CO} \\ \left[ \frac{f_{s,CR} - f_s}{f_{s,CR} - f_s} \right] \left[ \frac{f_{s,CR} - f_s}{f_{s,CR} - f_s} - 1 \right] \bullet f_d & \text{if } f_{s,CO} < f_s < f_{s,CR} \\ \infty & \text{if } f_s > f_{s,CR} \text{ (fluid flow ceases)} \end{cases} \quad (2)$$

where  $f_s$  is the solid fraction, a measure of the fraction of the total volume occupied by solid;  $f_{s,CO}$  is cohesive solid fraction beyond which the mean fluid viscosity does not rise, rather, the particles begin to interact with one another to cause solid-like behavior;  $f_{s,CR}$  is the critical solid fraction at which the sediment particles are completely bound together in a solid-like mass, and the drag coefficient  $K$  is infinite and fluid flow ceases.  $f_d$  is a drag factor.

The mean fluid viscosity  $\bar{\rho}$  is assumed to be a linear function of the sediment volume function:

$$\bar{\rho} = \rho_L + f_s(\rho_s - \rho_L) \quad (3)$$

where  $\rho_s$  and  $\rho_L$  are the densities of sediment particles and the liquid, respectively.

The motion of suspended sediment in FLOW3D is defined as follows:

$$\frac{\partial c_s}{\partial t} + \bar{u} \cdot \nabla c_s = D \nabla^2 c_s - \bar{u}_{lift} \cdot \nabla c_s - \bar{u}_{drift} \cdot \nabla c_s \quad (4)$$

where  $c_s$  is the local concentration of sediment, and  $D$  is a diffusion coefficient. In FLOW3D  $D$  is set as the molecular diffusion coefficient, or the turbulence diffusion coefficient multiplier;  $\bar{u}_{lift}$  and  $\bar{u}_{drift}$  are the local lifting and drifting velocities, respectively, and can be determined by

$$\bar{u}_{lift} = \alpha \bar{n}_s \sqrt{\frac{\tau - \tau_{crit}}{\bar{\rho}}} \quad (5)$$

and

$$\bar{u}_{drift} = \frac{f_L d^2}{18\mu} \frac{\nabla P}{\bar{\rho}} (\rho_s - \rho_L) \quad (6)$$

In (5),  $\bar{n}_s$  is the vector normal to the packed bed surface;  $\alpha$  is a dimensionless parameter that presents the probability that a particle is lifted away from the packed surface; its value is typically 1 or smaller. Note that, in practice, we find that  $\alpha$  often needs to be chosen larger than 1 to match the specific problems.  $\tau_{crit}$  is the minimum shear stress along the bed needed to cause lifting of the sediment particles, below which no erosion can occur. The flux is zero where the bed shear stress is less than the critical stress. At the surface of the packed bed of sediment, the fluid shear stress,  $\tau$ , acts to remove sediment; the amount eroded from the surface is a function of the fluid shear stress, the critical shear stress and the solid densities.

In (6),  $d$  is the mean sediment particle diameter, and  $\mu$  is the liquid viscosity.

Both UMETB and Jet tests are simulated by FLOW3D. The fundamental parameters for these two tests are set as below:

- (i) Turbulent model: Renormalized group (RNG) model.
- (ii) Gravity in Z-direction:  $-980 \text{ cm} / \text{s}^2$ .
- (iii) Average particle diameter of sand specimen (ASTM 20-30 ottawa sand): 0.071 cm; density:  $2.67 \text{ g} / \text{cm}^3$ ; critical shields number: 0.00043; and the angle of repose:  $22.0^\circ$ .

#### *Simulation of UMETB test*

FLOW3D v9.3 is employed in the following to simulate the above-mentioned experimental cases. Experimental observations show that, from Case A to D, the eroded profile is found quite uniform along the transverse section of the floodwall. Therefore, the 2D simulations can completely satisfy the need for our study. However, Case E cannot be simulated in the present paper.

The 2D simulations are conducted on the X-Z plan, and unit cell is set in Y direction. A nested meshing structure composed of two mesh parts viewing from X-Z plan for the problem is employed and shown in Figure 6. The first mesh is set for the plunge water inlet above the left sidewall, and the second part is set for the fluid and soil domain below. To match the physical conditions, the upper boundary condition for the first mesh part employs a constant pressure ( $= 0 \text{ Pa}$ ) with its height elaborately set up to keep the same outflow amount of the plunge jet as is in the experiments in Z direction, 28.9 k liter/hr.; the remaining lateral boundaries are, respectively,

set up as “Wall” in X-Z plan and “Symmetry” in the out-of-plan, i.e., X-Y direction. The second mesh part is set up for the fluid and soil area, and its upper and bottom boundary conditions are set as “Symmetry” and “wall” in Z direction, respectively; the two ends in Y direction are set as “Symmetry”, and the up-stream boundary in X direction is set as “wall” whereas the down-stream end is set “continulative”.

**Fig. 6 goes to here**

Figs. 7(a, b) – 10(a, b) are the predicted erosion profile in terms of maximum scour depth, and maximum scour depth vs. time for the four cases (A, B, C and D). Case E, with zigzag pattern blocks, could not be modeled due to the limitation of FLOW3D.

**Fig. 7 (a, b) to 10 (a, b) go to here**

Table 1 shows the comparison of FLOW3D predictions with the according experimental observations with the four above-listed cases.

**Table 1 goes to here**

From Table 1, we see that the experimental observations indicate that the order of the maximum erosion depth for the five cases is A, C, B, D and E. Therefore, from the test, it is concluded that Case D, i.e., the case with the acrylic strip arranged in an “L” type to the bottom of the plate, has most significant erosion-resistance capability. In contrast, the numerical results

indicate that the order of the maximum erosion depth for the four cases is A, B, C and D. It is seen that the numerical predictions, in general, compare well with the according experimental observations in terms of maximum erosion depth and its occurrence time.

Although there are somewhat discrepancies between the simulations and the tests, we conclude that the numerical results can correctly depict erosion process for the four cases. Next we will analyze the numerical results we obtain, and take lessons learned from the simulations.

Analyzing Figs. 7-10 and Fig. 11, we find that addition of the acrylic strip can change the inlet scouring jet in angle and magnitude. It is seen that, the higher is the acrylic strip set away from the sediment surface, the less is the magnitude and the angle of the inlet flow. The erosion depth is dependent on these two factors, plunge water inlet velocity and angle. It is obvious that an erosion-proof function mainly benefits from small scouring flow and small plunge angle since it reduced the vertical impinging energy and, therefore, leads to a weak erodibility.

**Fig. 11 goes to here**

Figs. 7(a)-10 (a) show that the plunge water inlet angle for Case A and B is both bigger than that of Case C and D, whilst the maximum velocity of scouring jet among these four cases does not differ significantly, therefore, this leads to such a result that the final eroded depth of Case A and B is bigger than that of Case C and D.

Comparing Figs. 9(a) and 10(a), we see that Case D using a “L” type is equivalent to increasing the vertical size of the acrylic strip. The outcome of this treatment is that the velocity of plunging water inlet for Case C is bigger than that of Case D, whilst the plunge water inlet

angle for the two cases are not significantly different, and, of course, this gives rise to such a result that the final eroded depth of Case C is bigger than that of Case D. Thus, we conclude that, first, the bigger is the angle of the inlet flow and its velocity, the bigger is erosion depth generated, and vice versa; second, using a “L” type material in a function of enhancing erosion-proof is superior to using a “box” type since it consumes less material while with the same erosion proof effect.

Practically, erosion location is another critical factor to be considered. The further the erosion area is generated away from the floodwall, the higher stability is with the floodwall. Figs. 7-10 reveal that, without any protective treatment like Case A, the erosion hole initiates from the very beginning below the floodwall, gradually develops to the right, and finally removes the sediment in the entire area. This leads to an easy failure of the floodwall system under the hydro-pressure from the left part of the sidewall. Case B generates an erosion area which is located in the furthest area away from the floodwall. This eroded area causes less effect onto the stability of the floodwall. Case C has an erosion area located in the middle of the sediment domain. Case D has two erosion areas which are located near and far away from the floodwall, respectively. It is obvious that the erosion area in Case B is the most desirable. To explore the mechanism of erosion area formation, we need to review the fundamental knowledge of sediment transportation. It is known that shear stress and fluctuating force control sediment scouring process. The former is associated with the property of the sediment whereas the latter is governed by the flow field. Jia et. al. (2001) indicates that fluctuating force is caused by the pressure fluctuation of the turbulent flow. The pressure fluctuation takes place near the stagnation point of plunging flow where the scour hole initiates and expands. Therefore, analysis of stagnation point of plunge water is critical to help understand the erosion area formation.

Figures 11 (a)-(d) show approximately the initial stagnation point locations for the four cases: Case A, 1.5 cm; Case B, 6.4 cm; Case C 4.2 cm; Case D, 5.01 cm. The time-marching erosion hole for each case is generated from the point, and gradually develops until the final erosion profile is formed. It is found that the final erosion locations are quite associated with the listed stagnation points. The length of the initial stagnation point location for the four cases is ordered in B, D, C and A, arranged in the same order as the finally predicted erosion locations of the according cases. As a conclusion, the outcome of the above numerical study indicates that an ideal floodwall protection device should be designed not only to help with reducing the erosion depth, but also to help removing the erosion area as far as possible away from the floodwall by means of enlarge the stagnation point of the impinging jet.

#### *Simulation of Jet test*

Fig. 12 depicts the predicted erosion profile of the Jet test (ASTM D5852) simulation with the velocity of jet inlet equal to 4.4 m/s. The simulated maximum erosion depth is 4.25 cm and the radius is 10 cm, whilst the according experimental data are 4.38 cm and 11 cm, respectively.

Fig. 13 depicts the predicted erosion profile for the UMETB test simulation with the velocity of jet inlet equal to -4.4 m/s.. The simulated maximum erosion depth is 4.54 cm and the radius is 11.17 cm, whilst the according experimental data are 5.60 cm and 14.8 cm, respectively.

The two experimental observations indicate that the UMETB test holds a deeper erosion depth and a wider eroded radius than that of the Jet test. Viewing from the simulations of these

two tests, we find that, although the numerical results of maximum erosion depth and the eroded radius values are of under estimation compared to the two according tests, the predicted eroded depth profile and erosion result tendency agrees well with each individual test. Hence, we conclude that the FLOW3D can correctly predict the jet test.

Erosion due to plunging water and nozzle jet are simulated using FLOW3D. The numerical prediction correctly predict erosion results in terms of maximum erosion depth & location versus time for plunging water erosion cases, and maximum erosion depth and eroded radius. It is concluded that FLOW3D is a reliable numerical tool for erosion investigations.

### **Acknowledgement**

This work was supported by the funding received under a subcontract from the Department of Homeland Security-sponsored Southeast Region Research Initiative (SERRI) at the Department of Energy's Oak Ridge National Laboratory, USA.

### **Conclusion**

Using the loosely packed C-109 Ottawa sand, the following conclusions can be made regarding the erosion behavior.

1. To simulate the plunging water erosion for levees in New Orleans floodwall and levee, a new erosion testing bed is designed and manufactured and named UMETB).

2. Using the UMETB, erosion characteristics of ASTM C-109 Ottawa sand was tested using the plunging water velocity 3.2 m/s to evaluate the erosion depth and time for floodwalls of several different surface conditions.
3. The results showed that adding engineered surface treatment, the erosion depth is substantially reduced (40% or more) and the erosion time is substantially increase (300% or more).
4. These experimental results agreed well with numerical results based on hydrodynamics simulation. From numerical simulation using FLOW3D, it is shown that the reduced erosion depth is due not only to the dissipated initial kinematic energy of plunging water but also to the decreased impinging angle when the water strikes the soil.
5. Based on results from UMETB in this paper, it is tentatively confirmed that the installation of the strips and blocks can be alternative methods to reduce or minimize the effects of erosion in the field. However, it is noted that reflecting the plunging water to an unprotected area may cause a secondary erosion, so that the use of these energy dissipating strips and blocks showed designed with careful theoretical and experimental validations.

## **References**

AlQaser, G. and Ruff, J. F. (1993). "Progressive failure of an overtopped embankment", *Proc., of the Hydraulic Engineering*, 1993, ASCE, New York, 1957-1962.

- ASTM. (1995). "Standard test method for erodibility determination of soil in the field or in the laboratory by the jet index method", *Annual Book of ASTM standard: Section 4, Construction*, ASTM, West Conshohocken, Pa., 04. 09.
- Brethour, J. (2006). "Modeling sediment scour", *FSI-03-TN62*, Flow Science, Inc.
- Briaud, J.-L., Ting, F., Chen, H.-C., Cao, Y., Gudavalli, R., Perugu, S., and Wei, G. (1999). "Sricos: Prediction of Scour Rate in Cohesive Soils at Bridge Piers", *J. Geo and Geoenv. Soc. Am.*, ASCE, 125(4), 237-246
- Briaud, J.-L., Ting, F., Chen, H.-C., Cao, Y., Han S.-W. and Kwak, K. (2001a). "Erosion Function Apparatus for Scour Rate Predictions", *J. Geo and Geoenv. Soc. Am.*, ASCE, 127(2), 105-113
- Briaud, J.-L., Chen, H.-C., Govindasamy, A. V. and Storesund, R. (2008), "Levee erosion by overtopping in New Orleans during the Katrina hurricane", *J. Geo and Geoenv. Soc. Am.*, ASCE, 134(5), 618-632
- Chen, Y. H. and Anderson, B. A. (1986), "Development of a methodology for estimating embankment damage due to flood overtopping", *Final Report, Simons, Li, and Assoc., Inc.*, Federal Highway Administration and Forest Service, Contact No. DTFH61-82-C-00104, SLA Project No. DC-FHA-01
- Coleman, S. E., Andrews, D. P., and Webby, M. G. (2002), "Overtopping breaching of non-cohesive homogeneous embankments", *J. Hydraul. Eng.*, 138 (9), 829-838
- Comoss, E J., Kelly, D. A., Leslie, H. Z. (2002), "Innovative erosion control involving the beneficial use of dredge material, indigenous vegetation and landscaping along the Lake Erie Shoreline", *Ecological Eng.*, 19(3), 203-210

- Dodge, R. A. (1988), "Overtopping flow on low embankment dams, Summary report of model tests", *Rep. No. REC-ERC-88-3*, U. S. Department of the Interior, Bureau of Reclamation, Denver, Colorado.
- Hanson, G.J. (1991), "Development of a jet index to characterize erosion resistance of soils in eastern spillways", *Trans.*, ASAE, 35(5), 2015-2020
- Hanson, G.J., and Robinson, K. M. (1993), "The influence of soil moisture and compaction on spillway erosion", *Trans.*, ASAE, 36(5), 1349-1352
- Hanson, G.J. and Cook, K.R. (2004), "Apparatus, test procedures, and analytical methods to measure soil erodibility in situ", *Applied Engineering in Agriculture*, ASAE, 20(4), 455-462
- Henderson, J. E. (1986), "Environmental designs for streambank protection projects", *Water Resource Bulletin*, JAWRA, 22(4), 549-558
- Hunt, S. L., Hanson, G. L., Cook, K. R., and Kadavy, K. C. (2004), "Breach widening observations from earthen embankment tests.", *Proc., American Society of Agricultural Engineers/Canadian Society for Engineering Annual Int. Meeting*, ASAE, Ottawa, Paper No. 042080
- Interagency Performance Evaluation Task Force (2007), "Performance evaluation of the New Orleans and Southeast Louisiana Hurricane Protection System," *U.S. Army Corps of Engineers*, <https://IPET.wes.army.mil>.
- Jia, Y.F., Kitamura, T. and Wang, S.S.Y. (2001), "Simulation of scour process in plunge pool of loose-bed material", *J. Hydro. Eng.*, March, 219-229.
- Moore, W.L., and Masch, Jr. F. D. (1962), "Experiments on the scour resistance of cohesive sediments." *J. Geophys. Res.*, 67(4), 1437-1449

Rohan, K., Lefebvre, G., Douville, S., and Milette, J. P. (1986), "A new technique to evaluate erosivity of cohesive material." *Geotech. Testing J.*, 9(2), 87-92

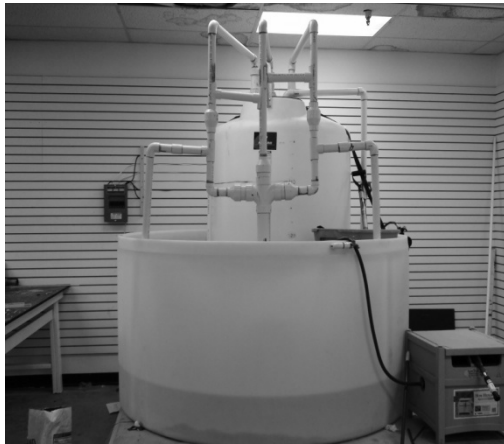
Shaw, C. F. (1929), "Erosion Pavement." *Geographical Review*, AGS, 19(4), 638-641

Table 1. Numerical predictions vs. the according experimental observations

	Case A		Case B		Case C		Case D		Case E	
	Num.	Exp.	Num.	Exp.	Num.	Exp.	Num.	Exp.	Num.	Exp.
Max. erosion depth (cm)	12.8	12.8	9.8	9.9	8.6	10.1	7.4	8.8	N.A.	8.4
Time (s)	1.7	1.65	3.0	2.66	2.8	2.66	3.0	2.83	N.A.	2.83



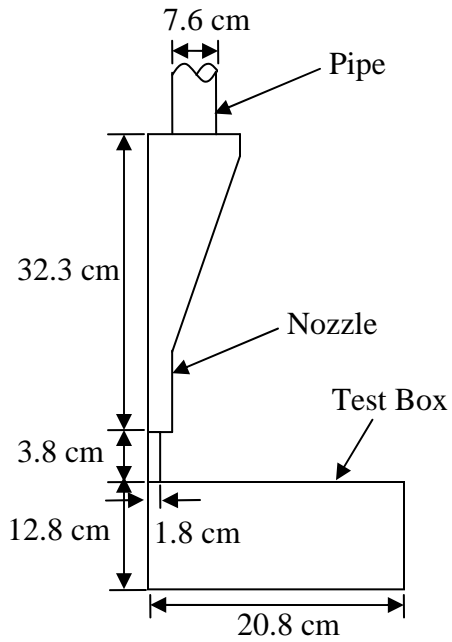
**Fig. 1.** Scouring caused by overtopping



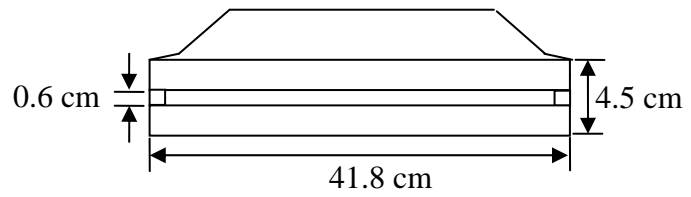
(a) View of outside UMETB



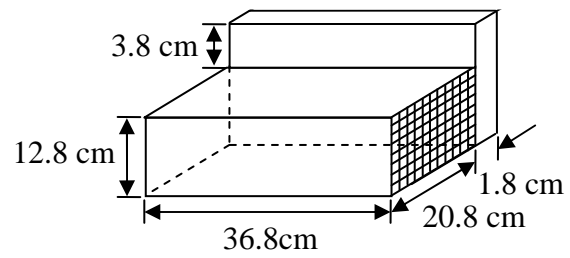
(b) View of inside UMETB



(c) Schematic of Nozzle and Test box set-up



(d) Schematic of Nozzle



(e) Schematic of Test box

**Fig. 2.** The UMETB test set-up

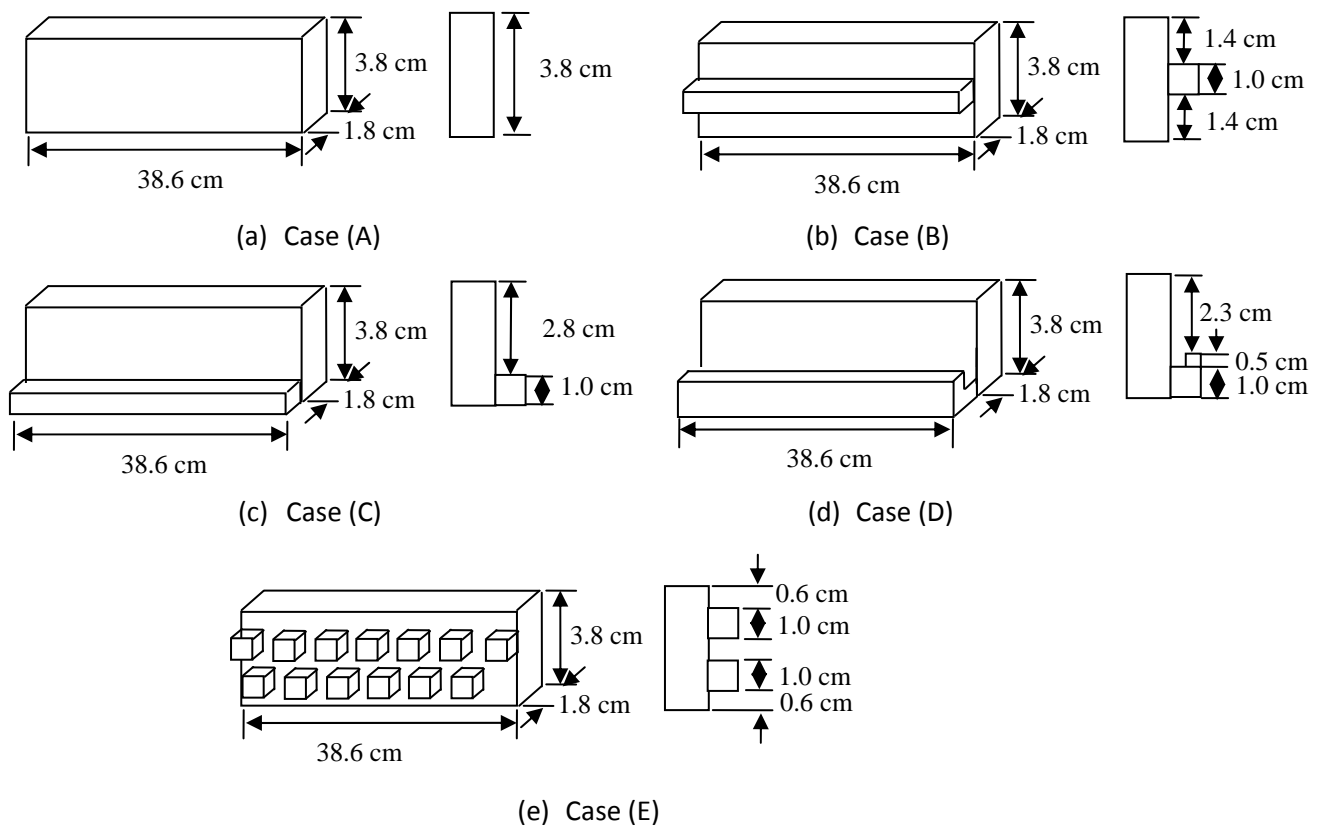
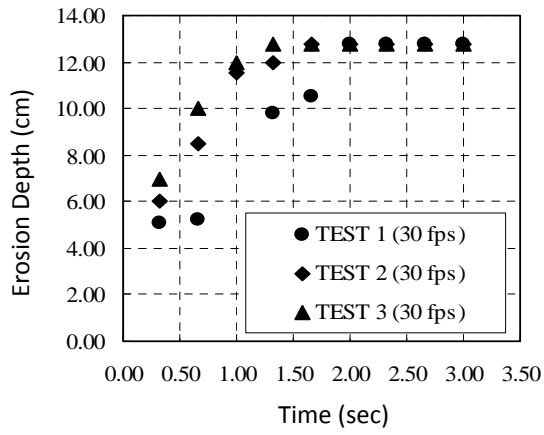


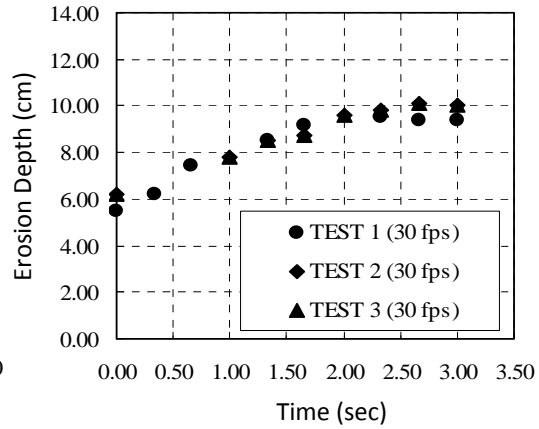
**Fig. 3.** Schematic shape of tested flood walls



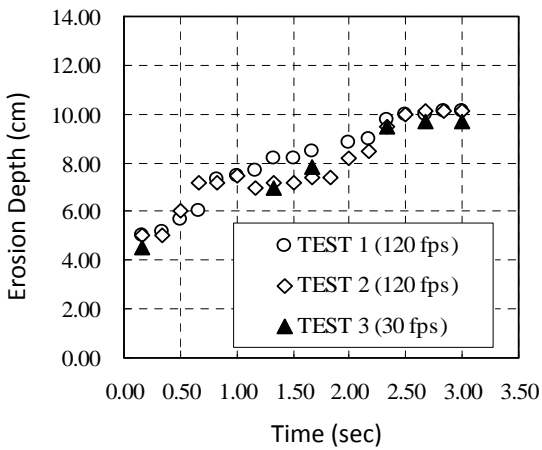
**Fig. 4.** 17<sup>th</sup> Street canal (Photo by Infrogmaton)



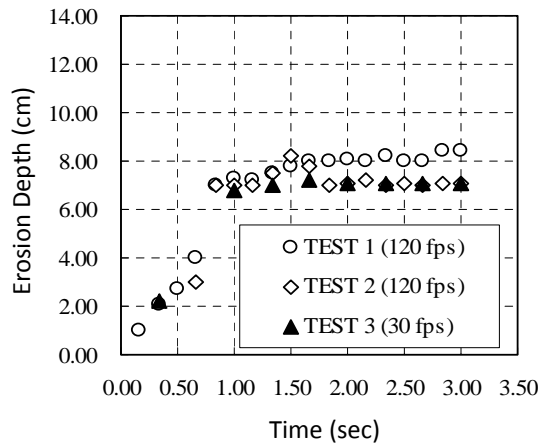
(a) Case (A)



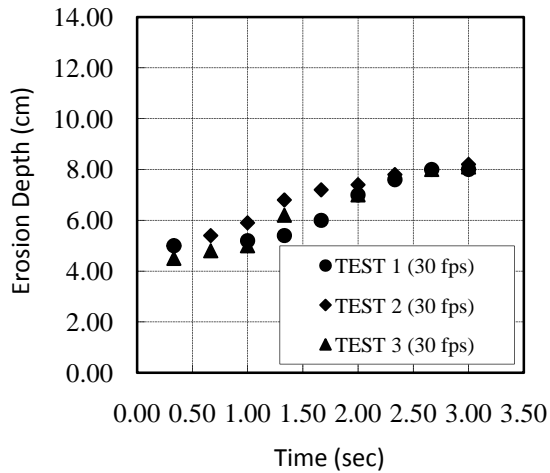
(b) Case (B)



(c) Case (C)



(d) Case (D)



(e) Case (E)

**Fig. 5.** Test results of case A, B, C, D, and E

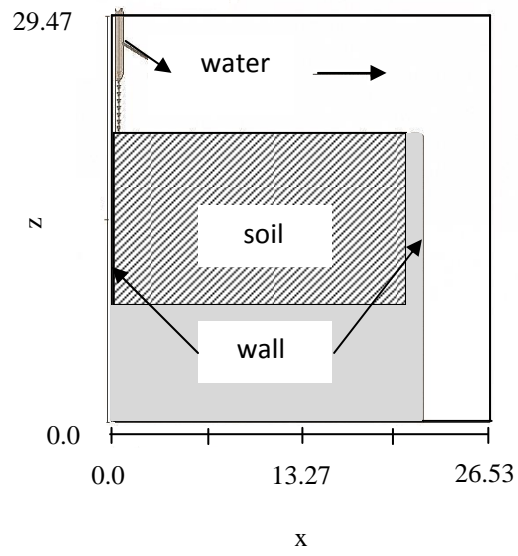
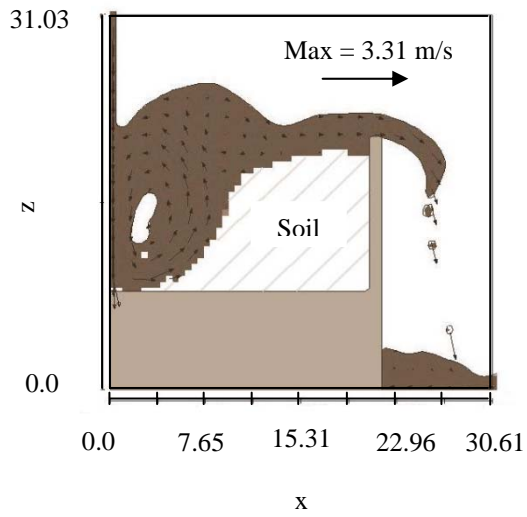
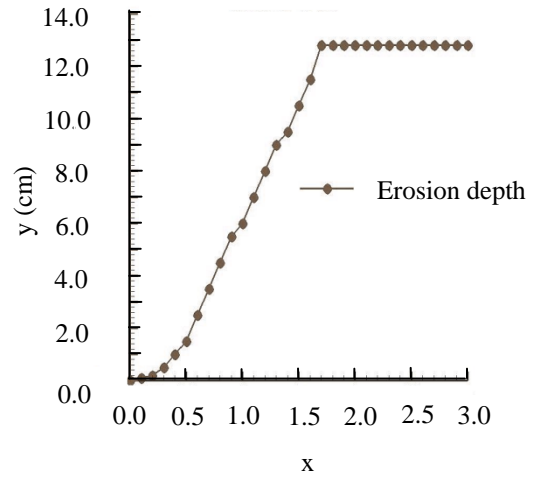


**Fig. 6.** Meshing system viewing from X-Z plan for simulating UMETB test

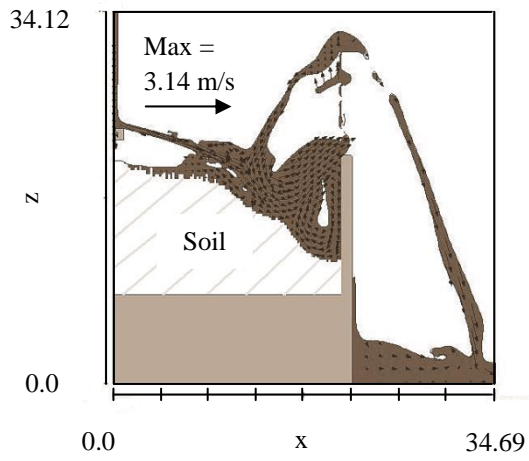


(a) Erosion profile at  $T=1.7$  s

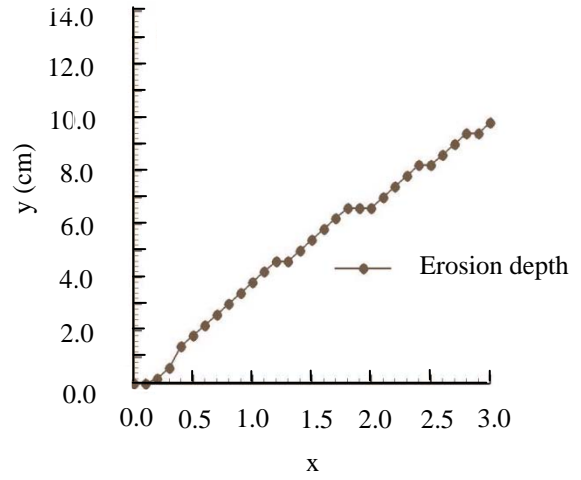


(b) Maximum scour depth vs. time

**Fig. 7.** Simulation of Case A

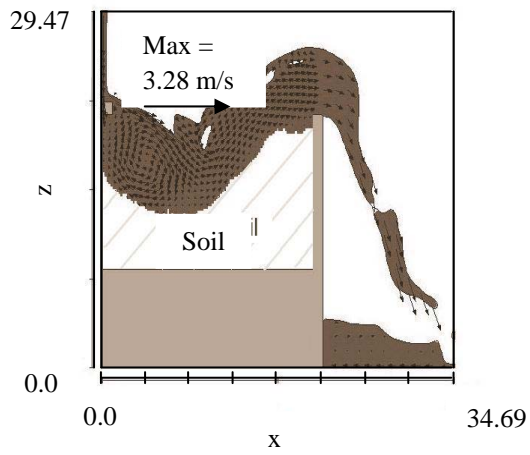


(a) Erosion profile at T=3.0 s

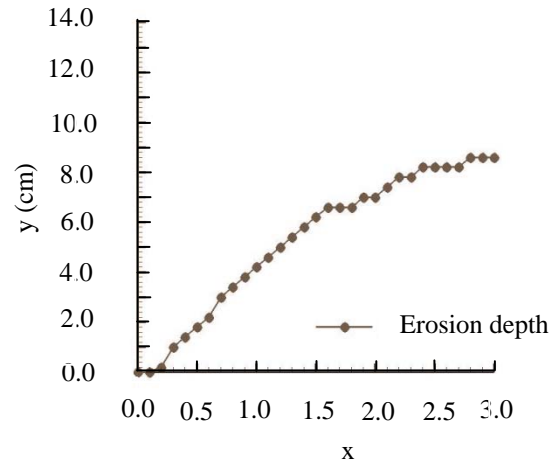


(b) Maximum scour depth vs. time

**Fig. 8.** Simulation of Case B

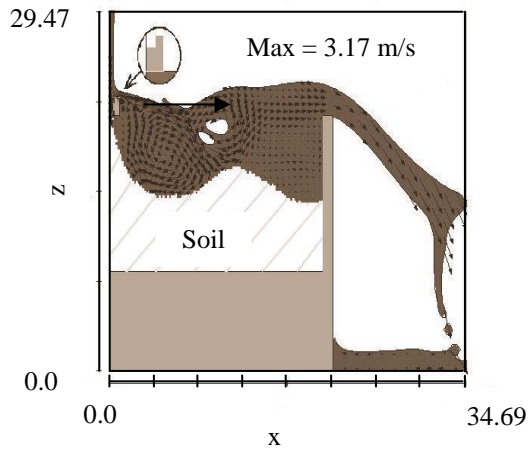


(a) Erosion profile at  $T=2.8$  s

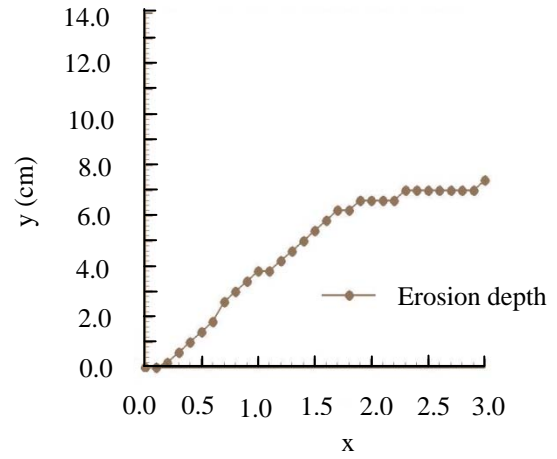


(b) Maximum scour depth vs. time

**Fig. 9.** Simulation of Case C

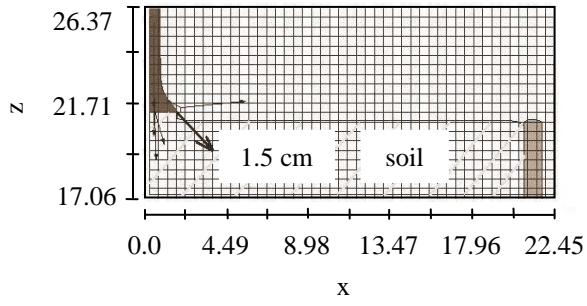


(a) Erosion profile at  $T=3.0$  s

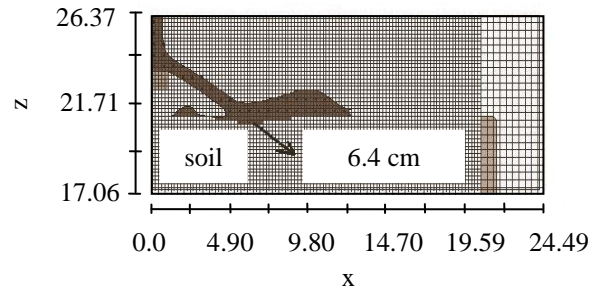


(b) Maximum scour depth vs. time

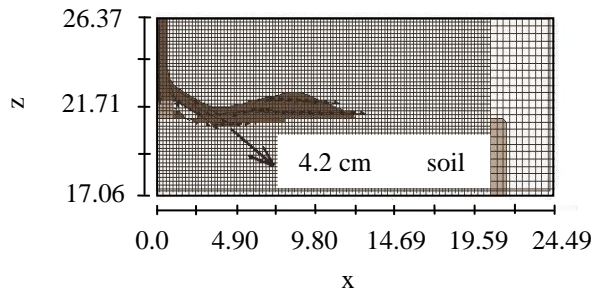
**Fig. 10.** Simulation of Case D



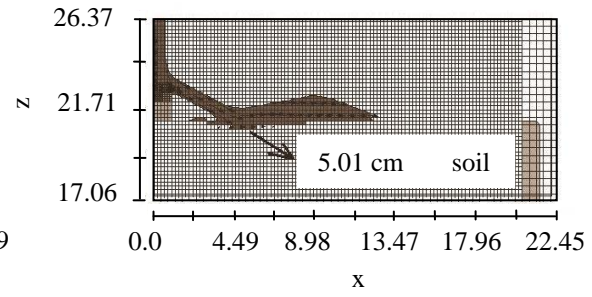
(a) Case A,  $T = 0.1$  s



(b) Case B

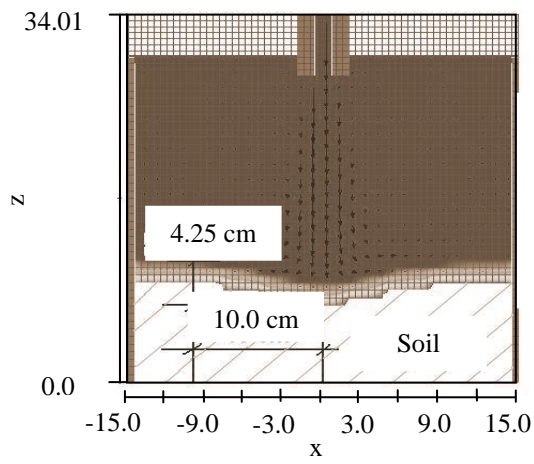


(a) Case C

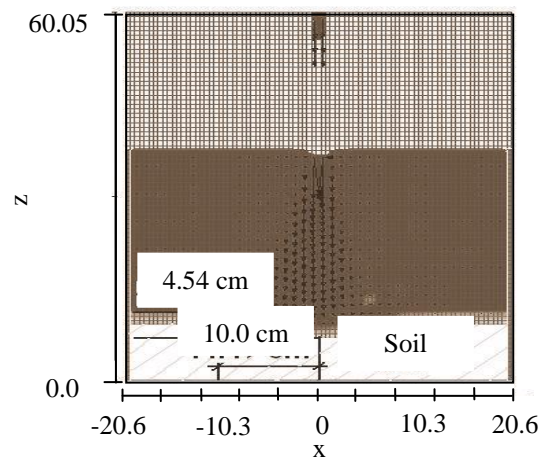


(b) Case D

**Fig. 11.** Simulation of incident plunge jet with (a) Case A, (b) Case B, (c) Case C, and (d) Case D.



(a) Jet test Jet test



(b) UMETB test

**Fig.12.** FLOW3D simulation result of Jet test.